Physics of Plasmas

On the expansion of non-ideal copper plasma into vacuum

Cite as: Phys. Plasmas **27**, 083519 (2020); https://doi.org/10.1063/1.5144684
Submitted: 09 January 2020 . Accepted: 28 July 2020 . Published Online: 18 August 2020

Dmitry Levko, Robert R. Arslanbekov, and Vladimir I. Kolobov

Physics of Plasmas ARTICLE scitation.org/journal/php

On the expansion of non-ideal copper plasma into vacuum

Cite as: Phys. Plasmas **27**, 083519 (2020); doi: 10.1063/1.5144684
Submitted: 9 January 2020 · Accepted: 28 July 2020 ·
Published Online: 18 August 2020

Dmitry Levko,[1,a)] Robert R. Arslanbekov,[1] and Vladimir I. Kolobov[1,2]

AFFILIATIONS

[1]CFD Research Corporation, 701 McMillian Way, Huntsville, Alabama 35806, USA
[2]Center for Space Plasma and Aeronomic Research, University of Alabama in Huntsville, Huntsville, Alabama 35899, USA

[a)]Author to whom correspondence should be addressed: dima.levko@gmail.com

ABSTRACT

The expansion of non-ideal copper plasma into vacuum is analyzed for the conditions typical for explosive electron emission in vacuum arcs. The computational model solves the Euler equations with an equation of state (EoS) for weakly non-ideal plasma, taking into account the ionization energy correction due to electron–ion Coulomb coupling. We have ascertained that the EoS has insignificant influence on the plasma expansion while the plasma properties and composition change drastically. Based on our simulation results, we discuss the validity of the "frozen" state theory often used in the vacuum arc plasma diagnostics.

I. INTRODUCTION

Plasmas expanding into vacuum or a background gas appear in many technological applications such as laser ablation,[1,2] physical vapor deposition,[3,4] electric propulsion,[5] inertial fusion,[6] hypersonic aircraft flow control, plasma assisted combustion,[7] etc.

Vacuum arc is one of the phenomena where plasma expansion appears naturally.[8] Today, the mechanism of vacuum arc ignition and operation is still under discussion.[8–13] Numerous studies testify that high-voltage vacuum breakdown occurs through micro-explosions at the cathode surface (see, for instance, Refs. 9, 10, 12, 14, and 15). These micro-explosions provide the gaseous media for a plasma plume forming the conductive channel. The micro-explosion mechanism can be explained as follows.[9,10,12] Micro-protrusions, which are always present at the metal surface, cause local enhancement of the electric field. When the electric field at the micro-protrusion tip exceeds the critical value ($\sim 2 \times 10^7$ V/cm), the electron field emission from the tip starts. The electric current heats the micro-protrusion causing thermo-field emission. If the emission current is large enough ($> 2 \times 10^8$ A/cm^2 for the copper cathode), a thermal runaway[9,16] occurs: the micro-protrusion temperature reaches the value of a few thousand Kelvin on the nanosecond time scale as a continuum phase transition metal-, liquid-, gas-plasma.[8] On such a short time scale, the electrode material cannot move, and after a few nanoseconds, a dense plasma cloud appears at the cathode surface. Very similar processes take place during the femtosecond laser ablation when a solid-to-plasma phase transition occurs on the sub-nanosecond time scale under the action of a laser pulse.[2]

The micro-explosions are accompanied by strong pressure gradients, which result in ion acceleration to supersonic velocities.[8,17–19] In Ref. 20, it was pointed out that measuring the ion velocity distribution function far from the explosion center can give useful information about the plasma state inside the explosion center. This method of plasma diagnostics is based on a theory of frozen state.[20] This theory assumes that the transition from dense equilibrium plasma to dilute non-equilibrium plasma occurs in an infinitely thin layer. In this layer, the plasma composition remains frozen and does not change during the plasma expansion.

The expansion of dense plasma from an explosive emission center was studied in numerous publications[21–24] using both hydrodynamic and particle-in-cell (PIC) models. Since the plasma density in the explosive emission center is close to solid density ($\sim 10^{28}$ m^{-3}),[8] the use of PIC models for the description of explosive emission center is questionable because the traditional PIC methods fail at high plasma densities, when the number of electrons within the Debye sphere is smaller than unity.[25] On the other hand, hydrodynamic models using ideal gas law for expanding plasmas miss important effects related to the non-ideal character of dense plasmas. In particular, the non-ideal gas equation of state (EoS) and the pressure ionization must be taken into consideration.[8,26]

As was pointed out in Ref. 27, vacuum breakdown occurs on the ion time scale, while the gaseous breakdown occurs on the electron time scale.[28] The disparity of time scales (electron, ion, and liquid) allows significant simplification of the computational models.

The liquid and electron time scales were explored in our previous publication.[28] In the present paper, we explore the processes that occur on the ion time scale. Here, we analyze the expansion of weakly non-ideal plasma into vacuum using a fluid model with a non-ideal plasma EoS. This EoS takes into account the contributions from both neutrals and charged species, and the ionization energy correction due to electron–ion Coulomb coupling. We consider only the gas dynamic model based on Euler equations and assume that the electrons, ions, and neutrals are in the local thermodynamic equilibrium (LTE) due to frequent interparticle collisions. By varying the gas temperature and pressure in a wide range, we analyze how the plasma non-ideality influences the plasma expansion dynamics.

II. COMPUTATIONAL MODEL

There are two regimes of plasma expansion,[20,29] which are characterized by the Damköhler number,[30,31] Da (see Fig. 1). This number is the ratio of the characteristic expansion time and the characteristic reaction time. At $Da \ll 1$, the plasma is in thermal non-equilibrium, while the ionization and recombination processes can be neglected. The latter is obtained because the species mean free paths are much larger than the typical length scales. Then, the charge states are said to be frozen and the ion charge distribution function is not changing during the expansion.[20] In the opposite case, at $Da \gg 1$, the charge state distribution is in the LTE. This means there is a balance between the ionization and recombination reactions due to frequent interparticle collisions. Indeed, the gas density in the explosive emission plasma center is equal to the solid density ($\sim 10^{28}$ m^{-3}). Due to such high gas density, the electron–neutral and the electron–ion collision frequencies are of the order of $\sim 10^{12}$–10^{14} s^{-1}. Therefore, all the species (electrons, ions, and neutrals) come to equilibrium on the time scale much shorter than the plasma expansion time (~ 1 μs).

In a more convenient form, the necessary condition for LTE is defined by the McWhirter criterion,[32,33]

$$n_e(\mathrm{m}^{-3}) > 1.6 \times 10^{18}\, \mathrm{T}^{1/2} (\Delta E_{nm})^3, \tag{1}$$

where T is the plasma temperature (in K) and ΔE_{nm} is the energy difference between levels n and m (in eV) which are in thermodynamic equilibrium.

In the LTE regime, all species are in thermodynamic equilibrium due to frequent interparticle collisions. As was shown, for instance, in Ref. 29, this regime is realized in the vicinity of the explosion center ($x < 1$ mm), where the gas density is close to the solid density. As the plasma expands, its density decreases. Then, the balance between ionization and recombination breaks, and the plasma comes to the non-equilibrium state. In the present paper, only the LTE plasma expansion is considered. The expansion of non-equilibrium plasma was analyzed, for instance, in Ref. 34 using the kinetic Vlasov equation solver. There are also numerous theoretical and hydrodynamic modeling studies devoted to the expansion of this plasma (see Refs. 35–37 and references therein).

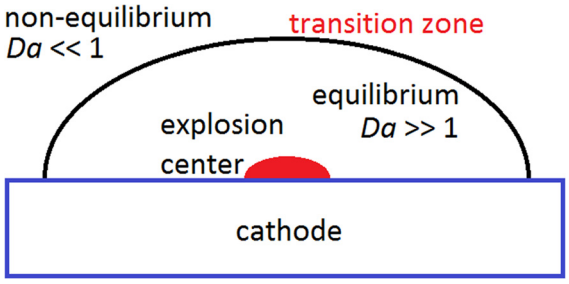

FIG. 1. Schematic representation of plasma expansion. Equilibrium and non-equilibrium regions are separated by a thin transition zone (bold black line).

The LTE plasma expansion into vacuum can be described by the system of one-dimensional (1D) Euler equations,[1]

$$\frac{\partial \rho}{\partial t} + \frac{\partial (\rho u)}{\partial x} = 0, \tag{2}$$

$$\frac{\partial (\rho u)}{\partial t} + \frac{\partial}{\partial x}\left(p + \rho u^2\right) = 0, \tag{3}$$

$$\frac{\partial}{\partial t}\left[\rho\left(E + \frac{u^2}{2}\right)\right] + \frac{\partial}{\partial x}\left[\rho u\left(E + \frac{p}{\rho} + \frac{u^2}{2}\right)\right] = 0. \tag{4}$$

Here, ρ is the density, u is the velocity, p is the pressure, and E is the internal energy. System (2)–(4) is solved for the density ρ, the momentum ρu, and the internal energy density ρE. A multi-dimensional, ideal-gas version of this model has been recently developed in Ref. 38. This model relies on a different compressible Euler solver and uses two Cu ion species, Cu^+ and Cu^{2+}. The model is thus applicable mainly to low-density, ideal plasma conditions, when the ionization into higher Cu states is not important. The 1D version of this model has been successfully validated against laser ablation experiments.

System (2)–(4) must be closed by the appropriate EoS. Dense plasma can be characterized by the degeneracy parameter, ξ, and the ideality parameter, γ.[39] The parameter ξ is the ratio of the plasma temperature and the Fermi energy, while γ is the ratio of the potential and kinetic energies of plasma particles. For the explosive emission plasma, one has $\xi_e < 1$ and $\xi_i < 1$, while $\gamma > 1$.[9] This means that such plasma can be described by the classical statistical theory, although there is a strong interaction between the electrons and ions.[39] Therefore, in our present model, we assumed that each plasma species is described by the ideal gas EoS resulting in the total pressure,

$$p = (1 + x_e)\rho kT/m, \tag{5}$$

while the internal energy density is defined by[1]

$$\rho E = \frac{\rho}{m}\left[\frac{3}{2}(1 + x_e)kT + \sum_{N=1}^{Z_{max}}\left(E_N \sum_{Z=1}^{Z_{max}} x_z\right)\right]. \tag{6}$$

Here, m is the atom mass, x_e is the electron fraction, x_z is the ion fraction, and Z_{max} is the maximum charge state of ions considered in the model. Also, $E_N = E_Q - \Delta E_Q$, where E_Q is the ionization threshold, and ΔE_Q is the ionization threshold lowering due to the electron–ion Coulomb coupling. Note that Eq. (5) is not an ideal gas EoS because the electron density defined as $\frac{\rho}{m}x_e$ is a non-linear function of temperature. We also impose the conservation of mass,[1]

$$x_0 + \sum_{Z=1}^{Z_{max}} x_z = 1, \tag{7}$$

and the charge conservation,

$$\sum_{Z=1}^{Z_{max}} Z x_z = x_e. \tag{8}$$

In Eq. (7), x_0 is the atom fraction. Within the LTE, the densities of plasma species are calculated using the system of Saha–Eggert equations,[1,20]

$$\frac{n_e n_{Q+1}}{n_Q} = \Lambda_B^{-3} \frac{2\Sigma_{Q+1}}{\Sigma_Q} \exp\left(-\frac{E_Q - \Delta E_Q}{kT}\right). \quad (9)$$

Here, $\Lambda_B = \frac{h}{\sqrt{2\pi m_e kT}}$ is the thermal de Broglie wavelength, h is the Planck constant, Q is the ion charge state, and Σ_Q are the ion partition functions. Equation (9) takes into account both the thermal and pressure ionizations.[40] The latter effect is obtained at high pressures, when the outer shells of atoms become compressed and finally disappear.[39] Energy ΔE_Q is calculated using the Debye–Hückel theory,[41]

$$\Delta E_Q = \frac{(Q+1)e^2}{4\pi\varepsilon_0(\lambda_D + \Lambda_B/8)}. \quad (10)$$

Here, e is the elementary charge, and λ_D is the plasma Debye length calculated by[41]

$$\lambda_D = \left\{\frac{\varepsilon_0 kT}{e^2\left(n_e + \sum_Q Q^2 n_Q\right)}\right\}^{\frac{1}{2}}. \quad (11)$$

Here, ε_0 is the permittivity of a free space, n_e is the electron number density, and n_Q are the ion number densities. The Debye–Hückel theory is valid until $\Delta E_Q < E_Q$.[41]

Equations (2)–(4) were discretized on a homogeneous numerical mesh with a cell size $\Delta x \approx 0.005$ mm. Depending on the pressure in the plume of expanding plasma, the time step was $\Delta t = 10^{-11}$–10^{-10} s in order to satisfy the Courant–Friedrich–Levy condition. The numerical solution of Eqs. (2)–(4) also requires the calculation of sound speed (see the Appendix).[42] The latter was found from

$$c_s^2 = \left.\frac{\partial p}{\partial \rho}\right|_E + \Gamma\frac{p}{\rho}, \quad (12)$$

where $\Gamma = \frac{1}{\rho}\left.\frac{\partial p}{\partial e}\right|_\rho$ is the Grüneisen coefficient.[43]

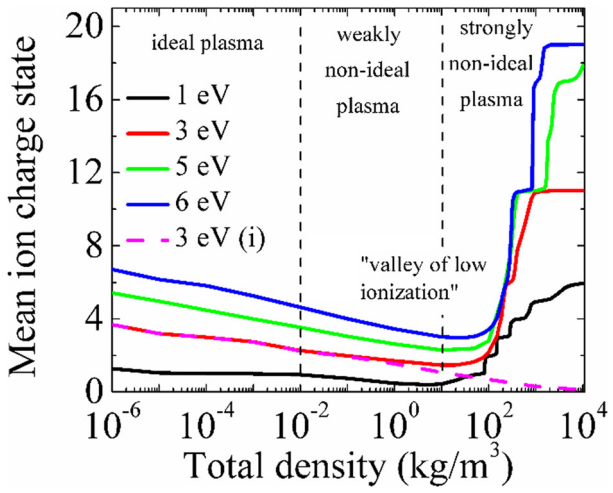

FIG. 2. Influence of the gas density on plasma composition for different values of the temperature. The dashed line shows the results obtained for 3 eV without accounting for the lowering of ionization energy.

III. GLOBAL ANALYSIS OF PLASMA COMPOSITION

This section presents the global analysis of the plasma composition. In this analysis, only the system of Eqs. (7)–(11) was solved. The temperature was considered as the external parameter. The copper (Cu) plasma consisting of 29 ions in the ground states was considered. The partition functions and the ionization energies were taken from Refs. 20 and 44, respectively. The gas density was varied from the rarefied flow conditions (10^{-6} kg/m^3) (Knudsen number of ~1–10) to the solid state (10^4 kg/m^3) conditions.

Figure 2 shows the influence of the total density and the temperature on the mean ion charge state, x_m. Similar results for various metals were obtained, for instance, in Refs. 20 and 45–47. In our model, $x_m = x_e$ because the total species density is kept constant.

The pink dashed line in Fig. 2 shows the mean ion charge state obtained for 3 eV without accounting for the lowering of ionization energy. One can see that below 10^{-2} kg/m^3, this curve coincides with

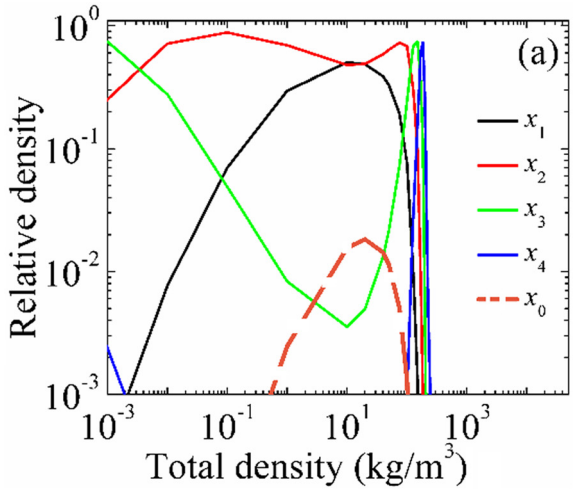

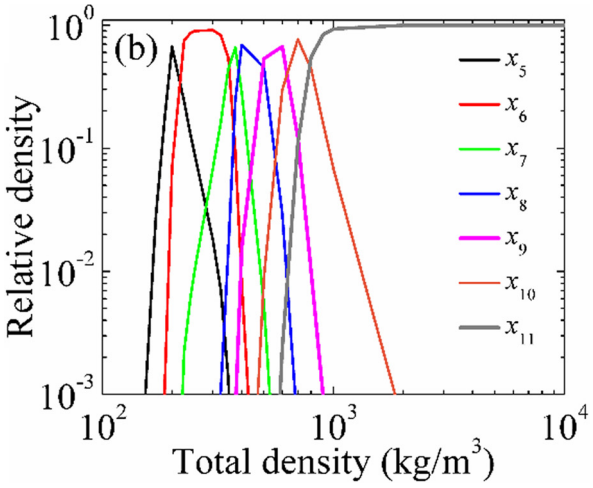

FIG. 3. Plasma composition as a function of gas density obtained for the temperature of 3 eV.

that obtained with account for the ionization energy correction. This means that this region on the diagram corresponds to ideal plasma. In the region $10^{-2}\,\mathrm{kg/m^3} < \rho < 10^{1}\,\mathrm{kg/m^3}$, both models predict a decrease in x_m for increasing density. However, the model with the ionization energy correction predicts a minimum of x_m at $\rho \sim 20\,\mathrm{kg/m^3}$, while another model predicts a monotonically decreasing x_m. In this model, only the thermal gas ionization is possible. Therefore, at extremely high gas density, there is not enough energy for the gas ionization. In Ref. 20, the region in the vicinity of the minimum of curve $x_m = x_m(\rho, T)$ was called the "valley of low ionization." In this region, the transition from weakly to strongly non-ideal plasma occurs.

The increase in the total plasma density leads to an increase in the role of the electron–ion Coulomb coupling, which results in a sharp increase in the mean ion charge. In this region, the main mechanism of the gas ionization is the pressure ionization.[40] Figure 2 shows that at high densities, the value of x_m saturates. One can conclude that the lower the temperature the lower the saturation value of x_m. In the asymptotic limit of very high pressures (not reachable for the conditions of our studies) and high temperatures, the plasma is fully ionized. It consists only of free bare nuclei and free electrons.

Figure 3 shows the plasma composition as a function of total density for $T = 3\,\mathrm{eV}$. These results were obtained using the model with accounting for the ionization energy lowering. One can see that there is a wide region where the ion with $Z = 2$ is the dominant. This region is typical for the laser ablation plasma.[1] In the region $10^{2}\,\mathrm{kg/m^3} < \rho < 10^{3}\,\mathrm{kg/m^3}$, there are several ions with the charge state $5 < Z < 11$ present in the plasma. However, there is always one dominant ion, and the densities of other ions are much smaller. At $\rho > 2 \times 10^{3}\,\mathrm{kg/m^3}$, only the ions with $Z = 11$ are present in the plasma. This result is explained by the large energy gap between the energy levels #11 and #12 (~100 eV).[44]

IV. ANALYSIS OF THE PLASMA EXPANSION

In this section, we analyze the plasma expansion in the vicinity of the valley of low ionization (see Fig. 2), where the Debye–Hückel theory is still valid. Initially, the simulation domain was divided into two parts. On the left, the initial gas pressure and density were, respectively, p_0 and ρ_0. On the right, the "vacuum" conditions were imposed (pressure $10^{-5}\,\mathrm{Pa}$ and density $10^{-3}\,\mathrm{kg/m^3}$). Below, the results of simulations for $p_0 = 5 \times 10^{9}\,\mathrm{Pa}$ and $\rho_0 = 10^{3}\,\mathrm{kg/m^3}$ are presented. These initial conditions are close to those obtained after the

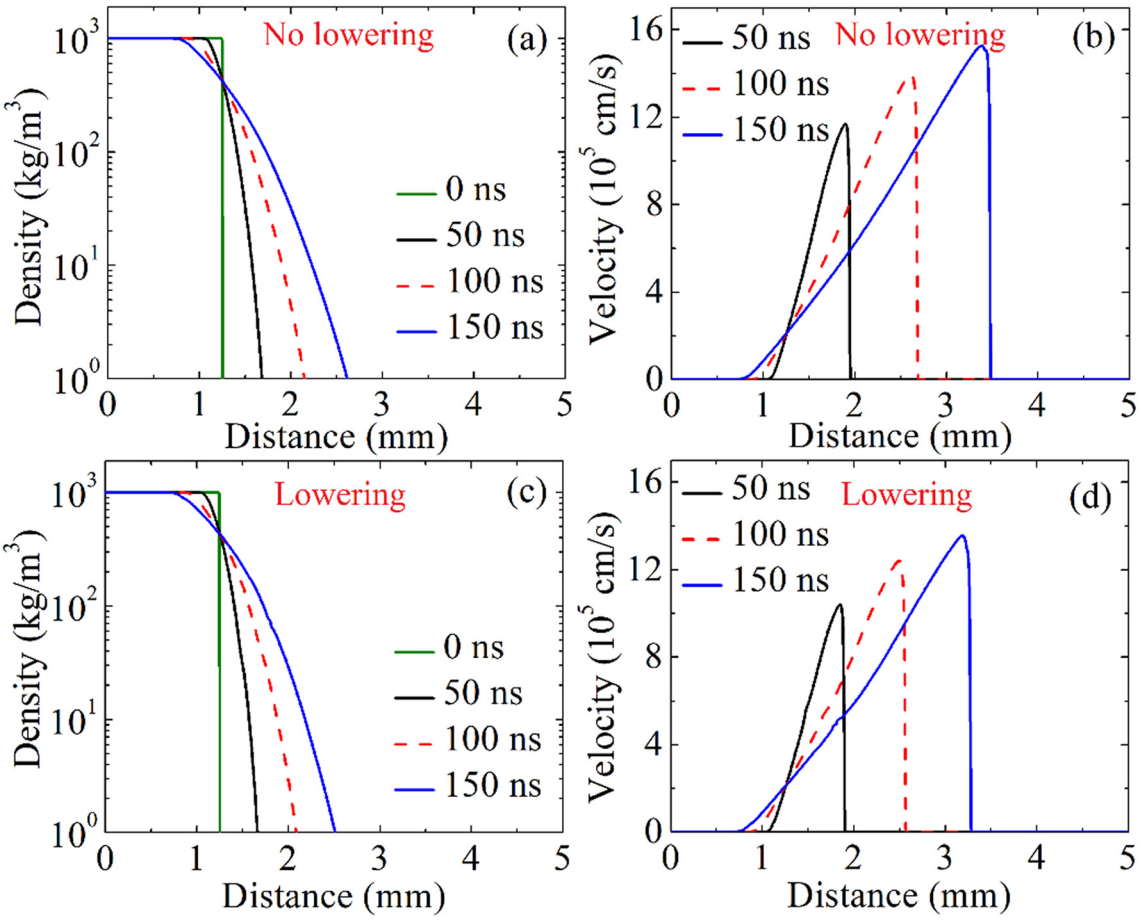

FIG. 4. (a) and (c) Density and (b) and (d) velocity without and with the accounting for the ionization potential lowering for the plume pressure of $5 \times 10^{9}\,\mathrm{Pa}$ and density $10^{3}\,\mathrm{kg/m^3}$.

micro-protrusion explosion.[9] Here, we do not consider the fast solid–liquid–gas-plasma continuum phase transition. As was shown in Refs. 9 and 16, this transition occurs at the nanosecond time scale due to the thermal runaway. This time is too short for the liquid motion, and the dynamics of this phase transition can be modeled by solving only the thermal heat balance equation.[9,16]

In the regime considered here, the pressure ionization is important, and one needs to consider the ionization energy correction defined by Eq. (10). For higher densities, plasma becomes strongly non-ideal, and the EoS (5)–(6) loses its validity. As it follows from Fig. 2, for $T< 6$ eV and for the total density in the range of 10^{-4}–10^{3} kg/m^3, the mean ion charge state does not exceed 6. Therefore, in this section, we consider the Cu plasma consisting only of six ions.

Figures 4–6 illustrate the main results of our simulations. These figures show a comparison between the models with and without accounting for the ionization potential lowering. One can conclude from Fig. 4 that both models predict very similar results. Both the gas density and the velocity profiles look similar. The comparison between Figs. 4(b) and 4(d) shows that the ideal plasma propagates faster than the non-ideal one. This difference can be explained by the small changes in the gas pressure obtained for both plasmas.

One can conclude from Figs. 4 and 5 that both the velocity and temperature increase at the leading edge of the expanding plasma. Since system (2)–(4) is isentropic,[48] the initial internal energy is gradually transformed into kinetic energy. The velocity increase follows from the density continuity Eq. (2), which shows that the decrease in density leads to the increase in the gas velocity.

Although the ionization potential lowering does not significantly influence the plasma expansion (Fig. 4), it does influence the plasma component content. Figure 5 shows the plasma temperature and the relative density of electrons, while Fig. 6 shows the densities of main ions. One can see that the accounting for the pressure ionization results in the decrease in the temperature of the explosive emission center, while the electron relative density increases. The comparison between Figs. 6(a) and 6(b) (see black lines) shows that x_e in the plume of weakly non-ideal plasma exceeds that in the plume of ideal plasma. This relation between T and x_e is obtained due to the way we set up the initial conditions. In our model, we fixed the initial pressure and

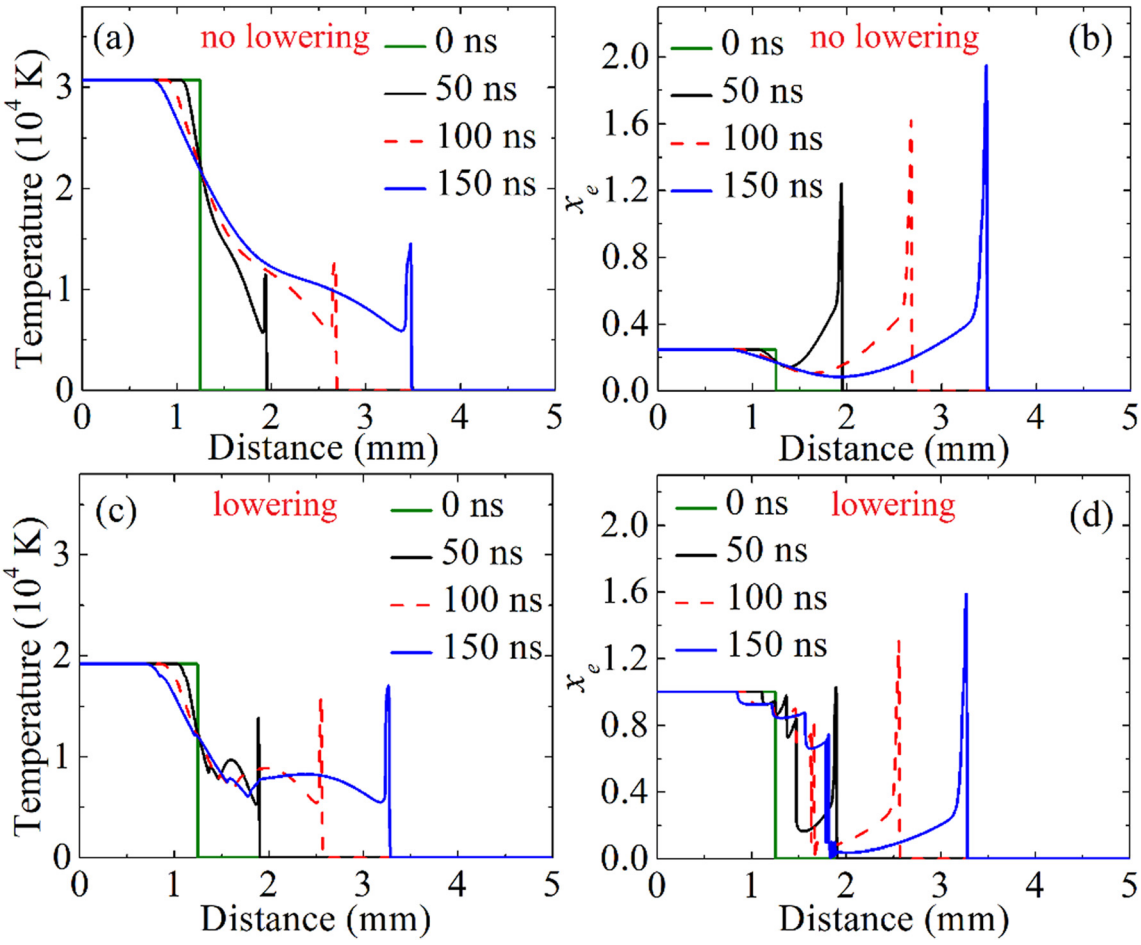

FIG. 5. (a) and (c) Temperature and (b) and (d) electron relative density without and with the accounting for the ionization potential lowering for the plume pressure 5×10^9 Pa and density 10^3 kg/m^3.

density in the explosion center. Therefore, as it follows from the EoS (5), the value of $(1 + x_e)T$ does not depend on the model. The lowering of the ionization potentials in the Saha–Eggert equations (9) results in the higher densities of plasma species. This results in the decrease in the gas temperature calculated by Eq. (6).

Both models give comparable values of both temperature and x_e at the leading edge of the expanding plasma (Fig. 5). In this region, both the gas pressure and the temperature are smaller than in the explosion center. The pressure drops to such an extent that the plasma becomes ideal at the leading edge.

Figure 6(a) shows that there are only ions Cu^+ in the explosion center of the ideal plasma. This is obtained because for the given gas density and temperature there is not enough energy for the thermal ionization with the generation of highly charged Cu ions. The accounting for the plasma non-ideality results in the appearance of the additional mechanism of the gas ionization, pressure ionization [see Fig. 6(b)]. This lowers the ionization energy thresholds in the Saha–Eggert equations (10) and results in the production of highly charged ions. Figure 6(b) shows that the non-ideal plasma of explosion center consists of four ions, Cu^+, Cu^{2+}, Cu^{3+}, and Cu^{4+}. Also, there is some small fraction of Cu^{5+} ions in the explosion center ($x_5 \sim 10^{-4}$). One can see that the primary ions are Cu^+. There is also a significant number of Cu^{2+}. The dependence of the average charge state of copper ions on the discharge current in the low-current vacuum arc was measured, for instance, in Ref. 49. The results of our simulations qualitatively agree with the experimental results for arc current less than 15 A. For higher currents, the experiments showed the Cu^{2+} ions as the dominant species.

The simulation results show that outside the explosion center, the gas pressure decreases. This reduces the electron–ion Coulomb coupling and the plasma becomes ideal. Since the pressure ionization is switched off, only singly charged Cu atoms are obtained between the explosion center and the leading edge. The densities of highly charged ions drop almost to zero along the distance $\sim 40\ \mu$m. Here, it is interesting to check the McWhirter criterion (1). For the conditions of Fig. 5, one obtains that for $x < 2.5$ mm, the critical electron density is $\sim 10^{23}$ m^{-3}, while for $x > 2.5$ mm, it is $\sim 10^{21}$ m^{-3} (see Fig. 7). Thus, at $x < 2.5$ mm, the plasma is in the LTE, while at $x > 2.5$ mm, it is non-equilibrium. In the latter region, our model is not valid and the electrostatic effects should be included.[35]

One can conclude from Figs. 7 and 5 that although the plasma species remain in the LTE at the distance of ~ 1 mm from the explosion center, the plasma composition changes drastically. This is obtained due to the switching off of the pressure ionization obtained during the plasma expansion. That is, there are two regions within the LTE region ($Da \gg 1$) with two different dominating ionization mechanisms. The theory of a frozen state[20,29] neglects the distinction between these two mechanisms. It assumes that the sudden freezing of the plasma component content happens when Damköhler number switches from $Da \gg 1$ to $Da \ll 1$. Then, one can relate the plasma species densities at the edge of the expanding plasma with their densities in the explosion center. However, as Anders pointed out in

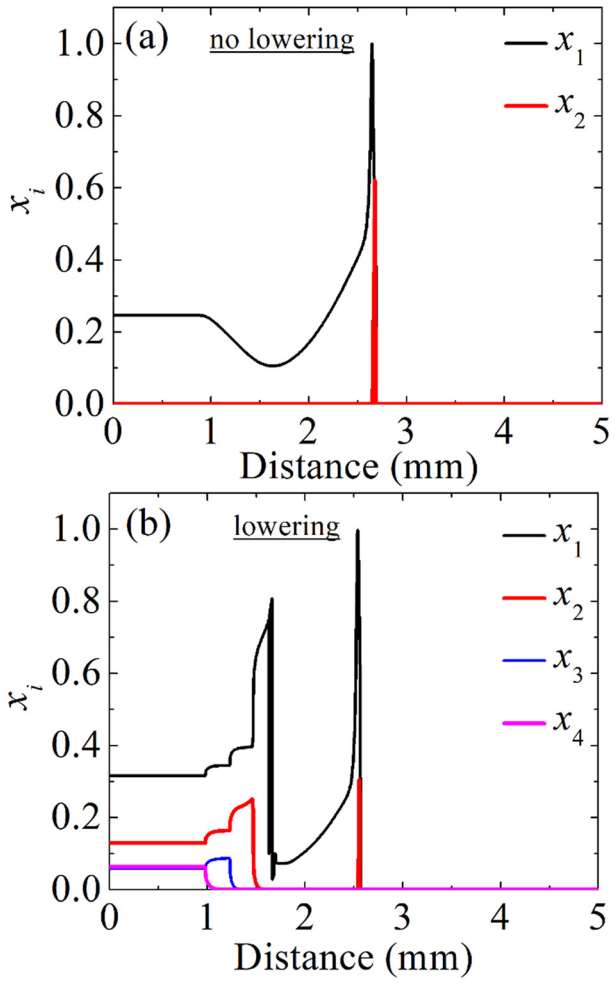

FIG. 6. Primary ion densities obtained at $t = 100$ ns (a) without and (b) with the accounting for the ionization potential lowering for the plume pressure 5×10^9 Pa and density 10^3 kg/m^3.

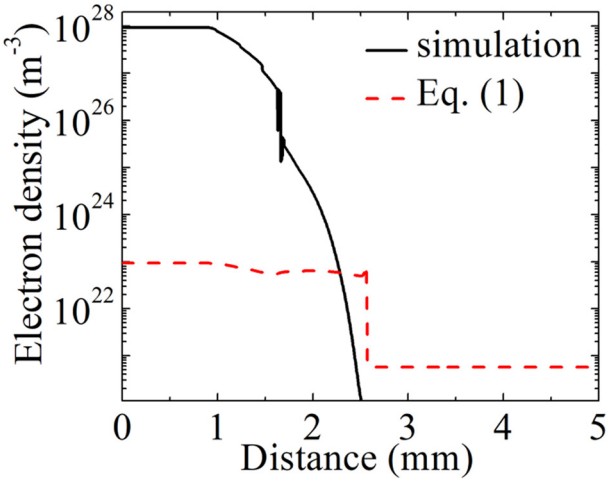

FIG. 7. The McWhirter criterion (1) and the electron number density obtained at $t = 100$ ns. $\Delta E_{nm} = 7.7$ eV was used in Eq. (1).

Ref. 29, the measured distributions of ions were broader than the calculated using the theory of a frozen state. One explanation is the non-sudden switching between the regions $Da \gg 1$ to $Da \ll 1$. Another explanation, reported in the present paper, is the existence of two different mechanisms of the gas ionization for the conditions of explosive emission plasma.

We also carried out the simulations for the explosion center pressure 5×10^8 Pa and density 10^2 kg/m^3. The obtained results were similar with the results shown above. The only difference was in the plasma composition. Namely, the decrease in the gas pressure results in the decrease in the energy correction factors ΔE_Q. Therefore, the mean ion charge state decreases when both p_0 and ρ_0 decrease. For further decrease in the gas density, as it follows from Fig. 2, the mechanism of thermal ionization becomes dominant, while the pressure ionization becomes less important. Our simulation results have also shown that the mechanism of plasma expansion qualitatively remains similar with that presented in this section for higher gas pressure and density.

V. SUMMARY

The expansion of weakly non-ideal plasma into vacuum was analyzed for the conditions typical to explosive electron emission. For our analysis, we have developed the computational model, which solves the Euler equations for gas dynamics, taking into account the equation of state for non-ideal plasma with the ionization energy correction due to the electron–ion Coulomb coupling.

We have obtained that the Coulomb coupling has insignificant influence on the plasma expansion. However, this effect is important for the plasma composition in the explosive emission center. We have also obtained that the leading-edge plasma is ideal and the ionization energy lowering is not substantial.

Our simulation results have shown that the plasma remains in the local thermodynamic equilibrium at distances of about 1 mm from the explosive emission center. However, the plasma expansion at this distance is accompanied by the transition from the pressure-ionization-dominant regime to the thermal-ionization-dominant regime, which leads to drastic changes of the ion composition within the LTE region.

ACKNOWLEDGMENTS

This work was supported by the DOE SBIR Project No. DE-SC0015746 and by the NSF EPSCoR Project No. OIA-1655280.

APPENDIX: NUMERICAL SOLUTION OF THE EULER EQUATIONS (2)–(4)

The Euler equations (2)–(4) were solved using the Godunov–Rusanov scheme adopted from Ref. 42. In conservative form, these equations are written as

$$\frac{\partial U}{\partial t} + \frac{\partial F}{\partial x} = 0, \tag{A1}$$

where $U = (\rho, \rho u, \rho E)^T$ and $F = (\rho u, \rho u^2 + p, u(\rho E + p))^T$. Then, the solution of Eq. (A1) can be found by the first order Godunov scheme,

$$U_i^{n+1} = U_i^n - \frac{\Delta t}{\Delta x}\left(F_{i+1/2}^n - F_{i-1/2}^n\right). \tag{A2}$$

The numerical flux is given by

$$F_{i+1/2} = F(U_i, U_{i+1}) = \frac{1}{2}\left(F_i + F_{i+1} - S_{i+1/2}(U_{i+1} - U_i)\right). \tag{A3}$$

Here, $S_{i+1/2} = \max\{|u_{i+1} + c_{s,i+1}|, |u_{i+1} - c_{s,i+1}|, |u_i + c_{s,i}|, |u_i - c_{s,i}|\}$, where $c_{s,i}$ is the speed of sound defined by Eq. (12). This scheme has good stability properties without needing to solve the Riemann problem.[42]

We tested this method against another solver developed in Ref. 50. Both methods give the same shock wave profiles, although there is small difference behind the shock wave, which is due to the numerical diffusion. Our simulation results have shown that the numerical diffusion obtained behind the shock wave using Saurel's method[42] is significantly reduced by decreasing the grid spacing. Although for two- and three-dimensional flows, this solution may be considered as unsatisfactory due to the influence on the computational time, it is acceptable for one-dimensional flows. In the present paper, we used Saurel's method because we found that Fuster's method[50] diverges for extremely high pressure and density differences in front of and behind the shock wave. At the same time, Saurel's method was developed to model explosions with extreme gradients of parameters.

DATA AVAILABILITY

The data that support the finding of this study are available from the author upon reasonable request.

REFERENCES

[1]A. Bogaerts, Z. Chen, R. Gijbels, and A. Vertes, Spectrochim. Acta Part B **58**, 1867 (2003).
[2]B. Rethfeld, D. S. Ivanov, M. E. Garcia, and S. I. Anisimov, J. Phys. D: Appl. Phys. **50**, 193001 (2017).
[3]A. Anders, *Handbook of Plasma Immersion Ion Implantation and Deposition* (Wiley-VCH, 2000).
[4]A. G. Nikolaev, E. M. Oks, K. P. Savkin, G. Y. Yushkov, and I. G. Brown, Rev. Sci. Instrum. **83**, 02A501 (2012).
[5]D. Goebel and I. Katz, *Fundamentals of Electric Propulsion* (John Wiley & Sons, 2008).
[6]S. Nakai and H. Takabe, Rep. Prog. Phys. **59**, 1071 (1996).
[7]M. Merino, E. Ahedo, C. Bombardelli, H. Urrutxua, and J. Pelaez, in 32nd International Electric Propulsion Conference, Wiesbaden, Germany, September 11–15 (2011).
[8]A. Anders, *Cathodic Arcs: From Fractal Spots to Energetic Condensation* (Springer, 2008).
[9]E. A. Litvinov, G. A. Mesyats, and D. I. Proskurovskii, Phys. Usp. **26**, 138 (1983).
[10]D. I. Proskurovsky, IEEE Trans. Plasma Sci. **37**, 1348 (2009).
[11]I. I. Beilis, IEEE Trans. Plasma Sci. **29**, 657 (2001).
[12]G. A. Mesyats, Phys. Usp. **38**, 567 (1995).
[13]H. T. C. Kaufmann, M. D. Cunha, M. S. Benilov, W. Hartmann, and N. Wenzel, J. Appl. Phys. **122**, 163303 (2017).
[14]Y. E. Krasik, J. Z. Gleizer, D. Yarmolich, V. Vekselman, Y. Hadas, and J. Felsteiner, IEEE Trans Plasma Sci. **36**, 768 (2008).
[15]I. Zhirkov, P. Polcik, A. Petruhins, S. Kolozsvári, and J. Rosen, J. Appl. Phys. **127**, 013301 (2020).
[16]D. V. Glazanov, L. M. Baskin, and G. N. Fursey, J. Tech. Phys. **59**, 60 (1989).
[17]R. Tanberg, Phys. Rev. **35**, 1080 (1930).
[18]B. Y. Moizhes and V. A. Nemchinskii, Sov. Phys. Tech. Phys. **25**, 43 (1980).
[19]C. Wieckert, Phys. Fluids **30**, 1810 (1987).

[20]A. Anders, Phys. Rev. E **55**, 969 (1997).
[21]S. A. Barengolts, G. A. Mesyats, and D. L. Shmelev, J. Exp. Theor. Phys. **93**, 1065 (2001).
[22]D. L. Shmelev and S. A. Barengolts, IEEE Trans. Plasma Sci. **41**, 1964 (2013).
[23]D. L. Shmelev, S. A. Barengolts, and M. M. Tsventoukh, IEEE Trans. Plasma Sci. **45**, 3046 (2017).
[24]E. V. Nefedtsev and A. V. Batrakov, J. Exp. Theor. Phys. **121**, 706 (2015).
[25]C. K. Birdsall and A. B. Langdon, *Plasma Physics via Computer Simulation* (IOP Publishing, Bristol, 1991), Chap. 1.
[26]D. L. Shmelev and E. A. Litvinov, IEEE Trans. Plasma Sci. **25**, 533 (1997).
[27]D. Levko, R. R. Arslanbekov, and V. I. Kolobov, in XXXIV ICPIG & ICRP-10, Sapporo, Hokkaido, Japan, July 14–19 (2019).
[28]D. Levko, R. R. Arslanbekov, and V. I. Kolobov, J. Appl. Phys. **127**, 043301 (2020).
[29]A. Anders, Plasma Source Sci. Technol. **21**, 035014 (2012).
[30]X. Sanchez-Vila, M. Dentz, and L. D. Donado, Geophys. Res. Lett. **34**, L10404, https://doi.org/10.1029/2007GL029410 (2007).
[31]S. Fogler, *Elements of Chemical Reaction Engineering*, 4th ed. (Pearson Education, Upper Saddle River, NJ, 2006).
[32]T. Fujimoto and R. W. P. McWhirter, Phys. Rev. A **42**, 6588 (1990).
[33]G. Cristoforetti, A. De Giacomo, M. Dell'Aglio, S. Legnaioli, E. Tognoni, V. Palleschi, and N. Omenetto, Spectrochim. Acta, Part B **65**, 86 (2010).
[34]V. Kolobov, R. Arslanbekov, and D. Levko, J. Phys.: Conf. Ser. **1225**, 012016 (2019).
[35]P. Mora, Phys. Rev. Lett. **90**, 185002 (2003).
[36]J. E. Allen and M. Perego, Phys. Plasmas **21**, 034504 (2014).
[37]Y. Hu and J. Wang, Phys. Rev. E **98**, 023204 (2018).
[38]S. B. Harris, J. H. Paiste, T. J. Holdsworth, R. R. Arslanbekovand, and R. P. Camata, J. Phys. D: Appl. Phys. **53**, 015203 (2019).
[39]V. E. Fortov, I. T. Iakubov, and A. G. Khrapak, *Physics of Strongly Coupled Plasma* (Oxford University Press, Oxford, UK, 2006), Chap. 1.
[40]W. Ebeling and W. Richert, Contrib. Plasma Phys. **25**, 431 (1985).
[41]W. Ebeling, W. D. Kraeft, and D. Kremp, *Theory of Bound States and Ionization Equilibrium* (Akademie-Verlag, Berlin 1976), Chap. 2.
[42]R. Saurel and R. Abgrall, SIAM J. Sci. Comput. **21**, 1115 (1999).
[43]R. Menikoff and B. J. Plohr, Rev. Mod. Phys. **61**, 75 (1989).
[44]*CRC Handbook of Chemistry and Physics*, 84th ed., edited by D. R. Lide (CRC Press, Boca Raton, Florida, 2003).
[45]D.-K. Kim and I. Kim, Phys. Rev. E **68**, 056410 (2003).
[46]K. Wang, Z. Shi, Y. Shi, J. Bai, J. Wu, and S. Jia, Phys. Plasmas **22**, 062709 (2015).
[47]Z. Fu, W. Quan, W. Zhang, Z. Li, J. Zheng, Y. Gu, and Q. Chen, Phys. Plasmas **24**, 013303 (2017).
[48]Y. Zel'dovich and Y. Raizer, *Physics of Shock Waves and High-Temperature Hydrodynamic Phenomena* (Dover, New York, 2002).
[49]Y. A. Zemskov and I. V. Uimanov, in 28th International Symposium on Discharges and Electrical Insulation in Vacuum, 23–28 September (2018).
[50]D. Fuster and S. Popinet, J. Comp. Phys. **374**, 752 (2018).